

Skin-Friction and Forced Convection from an Isothermal Rough Plate

Aubrey G. Jaffer
e-mail: agj@alum.mit.edu

Abstract

A novel analysis of the turbulence generated by steady flow along a self-similar roughness yields elegant new formulas for skin-friction coefficient and forced convection, both of which apply to isothermal plates having self-similar or periodic roughness in terms of root-mean-squared (RMS) height-of-roughness $\varepsilon > 0$:

$$f_C = \frac{1}{3 \ln^2(L/\varepsilon)} \quad \text{Nu} = \frac{\text{Re Pr}^{1/3}}{6 \ln^2(L/\varepsilon)} \quad \frac{L}{\varepsilon} \gg 1$$

Measurements of plates with periodic roughness by the author and by Pimenta, Moffat, and Kays (1975) support these formulas in the rough-turbulent regime.

Dimensional analysis indicates that for periodic isotropic roughness with period $L_S \ll L$, the least upper bounds for laminar and smooth-turbulent flow along the plate will be, respectively:

$$\text{Re}_L = 0.664^2 \frac{L L_S}{2 \varepsilon^2} \quad \text{Re}_S = 0.036^5 \frac{L L_S^4}{2^4 \varepsilon^5}$$

When $L_S/\varepsilon < 388$, the flow should transition directly from laminar to rough-turbulence at Re_L . When $L_S/\varepsilon > 388$, the flow should transition from laminar to smooth-turbulence at critical Reynolds number Re_L , and to rough-turbulence at Re_S .

Keywords: turbulence; skin-friction; profile roughness; forced-convection; critical Reynolds number

This research did not receive any specific grant from funding agencies in the public, commercial, or not-for-profit sectors.

Table of Contents

<i>Introduction</i>	2
<i>Prior Work</i>	2
<i>Rough-turbulence</i>	3
<i>Roughness</i>	4
<i>Self-Similar Profile Roughness</i>	5
<i>Vertical Roughness Travel</i>	6
<i>Skin-Friction and Forced Convection</i>	7
<i>Spectral Roughness</i>	8
<i>Periodic Roughness</i>	9
<i>Experimental Results</i>	11
<i>Fully Rough Regime</i>	12
<i>Transitional Rough Regime</i>	13
<i>Conclusions</i>	14
<i>Nomenclature</i>	15
<i>References</i>	16

1. Introduction

The skin-friction drag¹ of a rough surface is important to the fluid dynamics of vehicles and turbines. The related phenomenon of forced convection (from a rough surface) has application to modeling weather and the thermal behavior of buildings.

Section 2 reviews prior work on skin-friction from a rough plate.

Section 3 characterizes the turbulence resulting from flow along a rough surface.

Section 4 defines profile roughness, a roughness metric, and self-similarity for profile roughness functions.

Section 5 gives three examples of discrete self-similar profile roughness functions.

Sections 6 and 7 derive a formula for the skin-friction coefficient of a plate having self-similar roughness.

Section 8 characterizes the spectral properties of roughness profiles and gives a method for determining the effective repeat length from a roughness profile.

Section 9 derives Reynolds number bounds for applying the formulas for self-similar roughness to periodic roughness.

Sections 10, 11, and 12 present the results of testing plates with periodic roughness and find that they support the new theory in both the transitional rough and completely rough regimes.

2. Prior Work

In 1934 Prandtl and Schlichting published *Das Widerstandsgesetz rauher Platten (The Resistance Law for Rough Plates)*[1], which brilliantly infers a relation for skin-friction resistance for rough plates from their analysis of Nikuradse’s measurements of sand glued inside pipes (“sand-roughness”). In *Boundary-layer theory*[2] Prandtl and Schlichting give a formula for fully rough (large Re) total skin-friction coefficient for a rough flat plate in terms of its sand-roughness k_S and the characteristic-length L of the plate in the direction of flow:

$$c_f = \left(1.89 + 1.62 \log_{10} \frac{L}{k_S} \right)^{-2.5} \quad 10^2 < \frac{L}{k_S} < 10^6 \quad (1)$$

In *On the Skin Friction Coefficient for a Fully Rough Flat Plate*[3], Mills and Hang present a formula which they claim to be more accurate than the Prandtl-Schlichting formula (1) on the local skin-friction coefficient measurements from Pimenta, Moffat, and Kays[4]. Their corrected² total skin-friction coefficient formula is:

$$C_D = \left(2.035 + 0.618 \ln \frac{L}{k_S} \right)^{-2.57} \quad 750 < \frac{L}{k_S} < 2750 \quad (2)$$

In *Viscous Fluid Flow*[5], White gives a formula for fully rough local (not total) skin-friction coefficient:

$$C_f = \left(1.4 + 3.7 \log_{10} \frac{x}{k_S} \right)^{-2} \quad \frac{x}{k_S} > \frac{\text{Re}_x}{1000} \quad \Rightarrow \quad \frac{L}{k_S} > \frac{\text{Re}}{1000} \quad (3)$$

The roughness in the prior works is reported in Nikuradse’s sand-roughness metric k_S , the height of “coarse and tightly placed roughness elements such as for example coarse sand grains glued on the surface”. The utility of these formulas would be much greater if they were defined in terms of a roughness metric applicable to any surface. The most common traceable roughness metrics are root-mean-squared (RMS) and arithmetic-mean height-of-roughness. Both metrics were tried in this research. The formulas developed

¹ Skin-friction drag is the pressure opposing the flow due to viscous dissipation of the turbulence generated by flow along the surface.

² The Mills and Hang[3] published formula had a “6” where a “0” should have been in the first constant:

$$C_D = \left(2.635 + 0.618 \ln \frac{L}{k_S} \right)^{-2.57}$$

All of their measurement comparisons were of local skin-friction coefficient, which used a different formula. Figure 12 shows traces for both the corrected and uncorrected total formulas.

using the RMS height-of-roughness metric matched experimental data; the arithmetic-mean metric formulas did not.³

In *Skin-friction behavior in the transitionally-rough regime*[6], Flack, Schultz, Barros, and Kim measure skin-friction from grit-blasted surfaces in a duct. They write “The root-mean-square roughness height (k_{rms}) is shown to be most strongly correlated with the equivalent sand-roughness height (k_S) for the grit-blasted surfaces.”

Afzal, Seena, and Bushra in *Turbulent flow in a machine honed rough pipe for large Reynolds numbers: General roughness scaling laws*[7] fit 5.333 for the RMS to sand-roughness conversion factor and 6.45 for arithmetic mean to sand-roughness. 5.33 is used in Section 11 to compare formulas (1) and (2) with the present work.

3. Rough-turbulence

Forced flow along a flat plate with a rough surface is different in character from forced flow along a smooth surface because the peaks of roughness protrude through what would otherwise be a viscous sub-layer adjacent to the plate. Lienhard and Lienhard[8] teach: “Even a small wall roughness can disrupt this thin sublayer, causing a large decrease in the thermal resistance (but also a large increase in the wall shear stress).” The resulting boundary-layers will be much thinner than those arising from the same flow along a smooth plate.

Prandtl and Schlichting[1] assert that the plate’s height-of-roughness decreases relative to the depth of the boundary-layer growing along the plate in the direction of flow. This will not be true of a surface with self-similar roughness (as defined in Section 4). The ratio of the height-of-roughness to the characteristic-length of the plate being constant means that the height-of-roughness grows linearly with plate length (from its leading edge). The combination of repeated boundary-layer disruption with linear growth of the height-of-roughness results in the entire surface shedding rough-turbulence.

Although vortexes can arise in two-dimensional systems, turbulence is a three-dimensional phenomena. Its random velocity fluctuations must be isotropic at all but the coarsest length scales. In order that the random fluid velocities resulting from flow interactions with the plate roughness are not skewed, the roughness should be at least weakly isotropic; rotating the plate should not substantially affect the behavior of the system. A plate surface composed of parallel ridges and valleys would not meet this criterion.

Prandtl and Schlichting[1] split their analysis of turbulent flow into four regimes based on boundary-layer depth. The present analysis admits only three types of flow adjacent to a plate with isotropic periodic or self-similar roughness: laminar, smooth-turbulent, and rough-turbulent. Section 12 finds that the Prandtl-Schlichting transition points do not correspond to transitions in the measured data.

Section 9 gives Re bounds of rough-turbulent flow from periodic isotropic roughness.

Although laminar flow doesn’t appear, the measurements presented in Section 10 are successfully modeled using $f_C = 0.037 \text{Re}^{-1/5}$ for smooth-turbulence and new formula (14) for rough-turbulence. The measurements presented in Sections 11 and 12 are all for rough-turbulence, and modeled successfully by formula (14).

³ The “ $L/(6.45 \varepsilon)$ ” traces in the main graph of Figure 12 are computed using the arithmetic-mean metric.

4. Roughness

Let “profile roughness” be a function $z(x)$ where $0 \leq x \leq L$ is distance from the leading edge in the direction of flow. Functions being single-valued, neither tunnels nor overhangs are allowed.

Consider the roughness profile $z(x)$. Its mean height \bar{z} and root-mean-squared height-of-roughness ϵ are:

$$\bar{z} = \frac{1}{L} \int_0^L z(x) dx \quad \epsilon = \sqrt{\frac{1}{L} \int_0^L [z(x) - \bar{z}]^2 dx} \quad (4)$$

The roughness function $z(x)$ need not be continuous to be integrable. Local flow properties may not be well-defined anywhere. The present analysis focuses on the total skin-friction coefficient f_C .

A profile roughness function $z(x)$ has “self-similar roughness” with (integer) branching factor $n \geq 2$ if the RMS height-of-roughness of $z(x)$ over an interval $x_0 < x < x_n$ is n times the RMS height-of-roughness of $z(x)$ over each (evenly divided) sub-interval $x_\iota < x < x_{\iota+1}$ for $0 \leq \iota < n$ at a succession of scales converging to zero.⁴ A consequence of this definition of self-similar roughness is that the ratio of the length of the interval $L = x_n - x_0$ to its RMS height-of-roughness ϵ will be invariant over its succession of scales converging to zero.

Self-similarity is of interest because the skin-friction coefficient f_C , which will be formulated in Section 7, is a function of L/ϵ . If the roughness is self-similar, then L/ϵ and $f_C(L/\epsilon)$ will be constant over the span of the roughness profile.

In the three examples of self-similar profile roughness in Section 5, each roughness function is a permutation of the linear ramp $z(x) = x$ from $x = 0$ to $x = w$. Because the RMS height-of-roughness calculation depends only on the z values and not their relation to x , for all ramp-permutation profile roughness:⁵

$$\epsilon = \sqrt{\frac{1}{w} \int_0^w [x - w/2]^2 dx} = \frac{w}{\sqrt{12}} \quad (5)$$

This raises the question of whether a linear ramp, which is the identity permutation of a linear ramp, can produce rough-turbulence from a steady flow. A ramp doesn’t meet the isotropy requirement because a plate with a ramp profile in both directions has zero profile roughness perpendicular to the gradient.

⁴ Note that $z(x_\iota)$ values contribute to the interval height-of-roughness, but not to any sub-interval height-of-roughness.

⁵ The arithmetic-mean height-of-roughness of ramp-permutations is $w/4$.

5. Self-Similar Profile Roughness

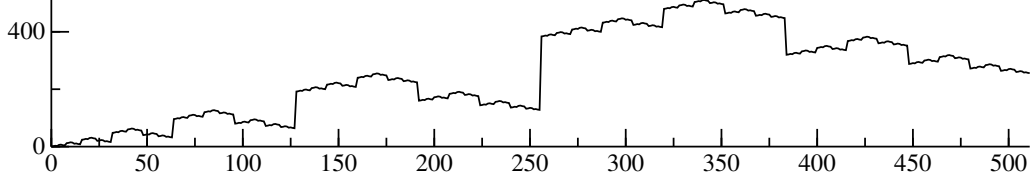


Figure 1 Gray-code profile roughness

The integer Gray-code sequence $G(x, w)$ with $0 \leq x < w = 2^l$ shown in Figure 1 has an RMS height-of-roughness $\epsilon = w/\sqrt{12}$ from equation (5) and is a self-similar roughness (bisected; $n = 2$) as seen by its recurrence:

$$G(x, w) = \begin{cases} x, & \text{if } w = 1; \\ w + G(w - 1 - (x \bmod w), w/2), & \text{if } \lfloor x/w \rfloor = 1; \\ G(x \bmod w, w/2), & \text{otherwise.} \end{cases} \quad (6)$$

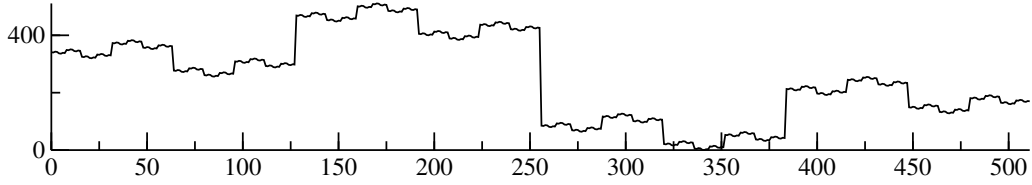


Figure 2 Wiggliest self-similar profile roughness

The integer sequence $W(x, w)$, which reverses at each bifurcation, produces the wiggliest possible self-similar roughness with $0 \leq x < w = 2^l$ and is shown in Figure 2. Being a ramp-permutation, it has an RMS height-of-roughness $\epsilon = w/\sqrt{12}$:

$$W(x, w) = \begin{cases} x, & \text{if } w = 1; \\ \lfloor x/w \rfloor w + W(w - 1 - (x \bmod w), w/2), & \text{otherwise.} \end{cases} \quad (7)$$

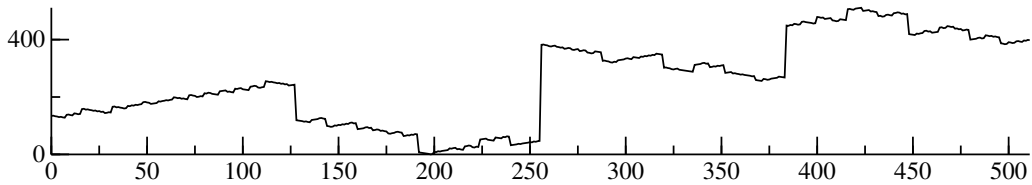


Figure 3 Randomly reversing bifurcation profile roughness

Figure 3 shows an integer sequence generated by recursive-descent with random reversing at each bifurcation. Being a ramp-permutation, it has an RMS height-of-roughness $\epsilon = w/\sqrt{12}$; its roughness is approximately self-similar.

There are 2^w distinct self-similar ramp-permutation roughness profiles. Profiles chosen randomly have w bits of sequence entropy ($w/2$ bits of Shannon entropy). There are only two distinct ramp profiles and only two distinct wiggliest profiles; their sequence entropies are 1 bit.

6. Vertical Roughness Travel

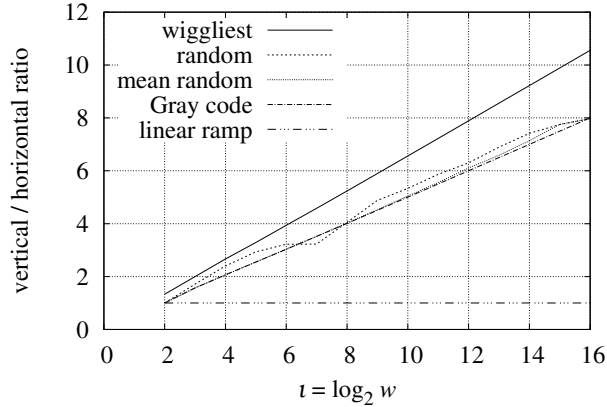


Figure 4 Travel along profile roughness

In order to convert some of the flow to rough-turbulence, parcels of fluid must move in directions not parallel to the bulk flow. Such movement could result from deflection of flow by the vertical spans of discrete profile roughness; the amount of turbulence produced would grow with the height-of-roughness.

For integer ramp-permutation roughness profile $Y(x, w)$, the sum of the lengths of all horizontal segments is $w - 1 = 2^l - 1$. The sum of the absolute value of the length of each vertical segment is:

$$\sum_{x=0}^{2^l-2} |Y(x, 2^l) - Y(x+1, 2^l)| \quad (8)$$

If a parcel of fluid were to trace the ramp-permutation roughness profile $Y(x, w)$ from $x = 0$ to $x = w - 1$, then $w - 1$ is the horizontal distance it would travel, while formula (8) is the vertical distance.

Shown in Figure 4 is the vertical to horizontal travel ratio versus l , the base-2 logarithm of w . The slope is 1/2 for the Gray-code and random-reversal cases, but 2/3 for the wiggliest roughness W . And the vertical segments in Figure 2 are indeed longer than the vertical segments in Figures 1 and 3.

A wiggliest roughness profile $W(x, w)$ is an extreme case; it reverses vertical direction at each increment of x . For each wiggliest roughness profile there are many more random bifurcation roughness profiles. Going forward, $W(x, w)$ will be excluded as an outlier.

From Figure 4 the vertical to horizontal travel ratio for the Gray-code and random-reversal sequences deviates little from:

$$\frac{l}{2} = \frac{\log_2 w}{2} \quad (9)$$

Formula (9) is unbounded as w increases. At some scale of w , vertical fluid movement by a distance of L/w will induce negligible turbulence. The argument to \log_2 must be dimensionless. $\log_2(\epsilon/L)$ is always negative because $\epsilon \ll L$; $\log_2(L/\epsilon)$ is positive, but inverts the sense of formula (9). Letting $w = L/\epsilon$, the ratio of vertical to horizontal travel is then:

$$\frac{2}{\log_2(L/\epsilon)} \quad (10)$$

From equation (5), the maximum peak-to-valley height is $\sqrt{12}$ times the RMS height-of-roughness ϵ . So the vertical to horizontal ratio should be scaled:

$$\frac{1}{\sqrt{12}} \frac{2}{\log_2(L/\epsilon)} = \frac{1}{\sqrt{3} \log_2(L/\epsilon)} \quad (11)$$

In *Self-Similar Processes Follow a Power Law in Discrete Logarithmic Space*[9] Newberry and Savage demonstrate that some self-similar systems which are modeled using continuous power-law probability distributions (such as the Pareto distribution) are better modeled using discrete power-law distributions.

The present work uses their idea in reverse. Conversion of flow into turbulence by contact with discrete self-similar roughness having been modeled above, the turbulence generation by a random self-similar roughness will be inferred using a random variable.

The base-2 logarithm is an artifact of the discrete roughness functions from Section 5. The analogous mean field theory is to treat $Z = |\Delta Y|$ as a continuous random variable having a Pareto distribution where the frequency of Z is inversely proportional to Z^2 :

$$1 \left/ \left[\int_{\epsilon}^L \frac{\sqrt{3} Z}{Z^2} dZ \right] \right. = \frac{1}{\sqrt{3} \ln(L/\epsilon)} \quad (12)$$

In this generalization of formula (11) to isotropic self-similar roughness, the surface height-of-roughness ϵ , defined in (13), is used in formula (12) instead of the profile height-of-roughness ϵ .

$$\bar{z} = \frac{1}{A} \int_A z dA \quad \epsilon = \sqrt{\frac{1}{A} \int_A [z - \bar{z}]^2 dA} \quad (13)$$

7. Skin-Friction and Forced Convection

For a rough flat surface subjected to a steady flow parallel to its surface which is sufficiently fast to generate rough turbulence, the skin-friction drag is the pressure opposing the flow due to viscous dissipation of that turbulence.

The skin-friction coefficient f_C is the ratio of the shear stress τ , which is primarily the skin-friction drag when $L/\epsilon \gg 1$, to the flow's kinetic energy density $\rho v^2/2$, where v is the bulk flow velocity and ρ is the fluid density.

$$f_C = \frac{\tau}{\rho v^2/2} \quad (14)$$

f_C is dimensionless; both τ and $\rho v^2/2$ have units of pressure, $\text{kg}/(\text{m} \cdot \text{s}^2)$.

Scaling by the vertical to horizontal travel ratio from formula (12) converts a horizontal velocity v to a friction velocity v^* , from which τ is derived:⁶

$$v^* = \frac{v}{\sqrt{3} \ln(L/\epsilon)} \quad \tau = \frac{\rho v^{*2}}{2} = \frac{\rho v^2}{6 \ln^2(L/\epsilon)} \quad \frac{L}{\epsilon} \gg 1 \quad (15)$$

Combining equations (15) and (14) produces a formula for f_C dependent only on L/ϵ :

$$f_C = \frac{1}{3 \ln^2(L/\epsilon)} \quad \frac{L}{\epsilon} \gg 1 \quad (16)$$

Figure 12 plots f_C over four decades of L/ϵ .

The Chilton and Colburn J-factor analogy (17) relates friction factors to turbulent forced convective heat transfer.

$$\text{Nu} = \frac{f_C}{2} \text{Re Pr}^{1/3} \quad (17)$$

Combining equation (17) with equation (16) produces a formula for forced convection:

$$\text{Nu} = \frac{\text{Re Pr}^{1/3}}{6 \ln^2(L/\epsilon)} \quad (18)$$

⁶ Prandtl and Schlichting[1] calculate τ as $\tau = \rho v^{*2}$, not $\tau = \rho v^{*2}/2$. This results in Prandtl-Schlichting c_f being twice f_C of the present work.

8. Spectral Roughness

There is an deep connection between the discrete Fourier transform X_j of a discrete roughness profile $Y(x, w)$ and its RMS height-of-roughness ϵ :

$$X_j = \sum_{x=0}^{w-1} Y(x, w) e^{-2\pi i j x/w} \quad \epsilon = \sqrt{\frac{1}{w} \sum_{j=1}^{w-1} |X_j|^2} \quad (19)$$

Note that the constant term, X_0 (which is the mean value of Y), is not included in the sum for ϵ .

Because each discrete Fourier coefficient is a Riemann sum over rectangles, the discrete Fourier transform underestimates the area under the integrals and introduces a phase shift. The corrected spectrum is:

$$S_j = X_j \frac{w}{2j} \sin \frac{\pi j}{w} \exp \frac{\pi i j}{w} \quad 0 < j \leq \frac{w}{2} \quad (20)$$

This correction is not appropriate for physical roughness measurements.

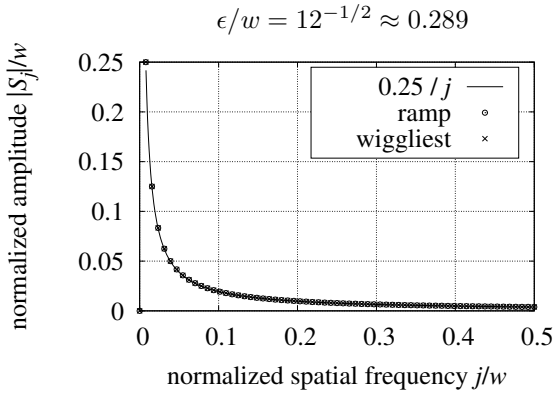


Figure 5 wiggliest and ramp spectra

Figure 5 shows the $|S_j|/w$ spectra of the wiggliest (in Figure 2) and ramp profiles. The amplitudes of the wiggliest and ramp spectra are identical; the difference in their profiles is encoded in the phase of the complex-valued S_j ; the ramp phases are all 90° or all -90° , while the wiggliest phases are an unequal mixture of $+90^\circ$ and -90° .

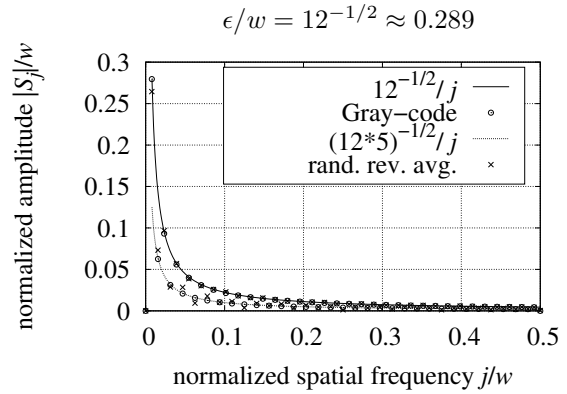


Figure 6 Gray and random spectra

Figure 6 shows the $|S_j|/w$ spectrum of the Gray-code roughness profile (from Figure 1) and the average of the amplitudes of the Fourier spectra of 187 instances of 128-point random-bifurcation profiles. The similarity between these spectra indicates that Gray-code roughness is representative of self-similar ramp-permutation roughness. The phases of the Gray-code spectrum are evenly distributed among 0° , 180° , 63.43° , and 116.57° (which is the dihedral angle of the dodecahedron).

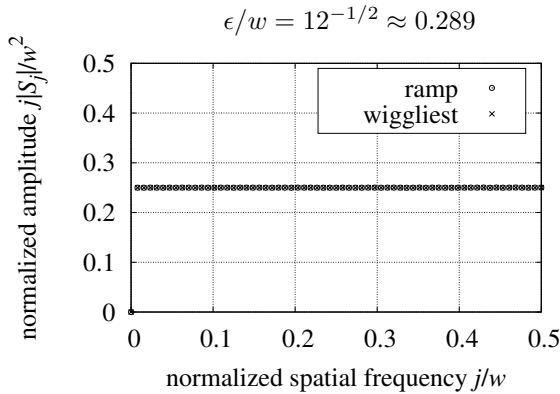


Figure 7 wiggliest and ramp spectra

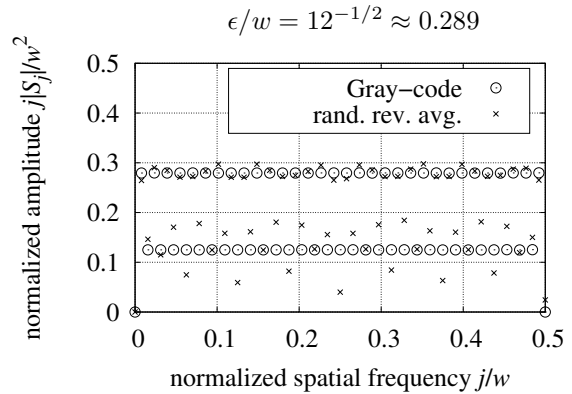


Figure 8 Gray and random spectra

The similarity length scale is proportional to w/j . In order to show the spectral structure of roughness across scale, $j|S_j|/w^2$ normalizes the spectrum relative to S_{j_P} , where j_P is the index of the largest $|X_j|$.

$j|S_j|/w^2$ is more appropriate to roughness than S_j/w because $j|S_j|/w^2$ is proportional to the vertical roughness travel in Section 6.

Figures 7, 8, and 10 show $j|S_j|/w^2$ spectra corresponding to the S_j/w spectra in Figures 5, 6, and 9 respectively. The traces for the ramp, wiggliest, and Gray-code profiles in Figures 7 and 8 show that these profiles are self-similar; the amplitudes repeat across the spatial frequencies. It is remarkable that the ramp and wiggliest profiles have identical spectral amplitudes given how differently these two profiles appear. But both are ramp-permutation outliers not covered by the present theory.

In Figure 8 the ratio between the two non-zero $j|S_j|/w^2$ levels for Gray-code is $\sqrt{5}$.

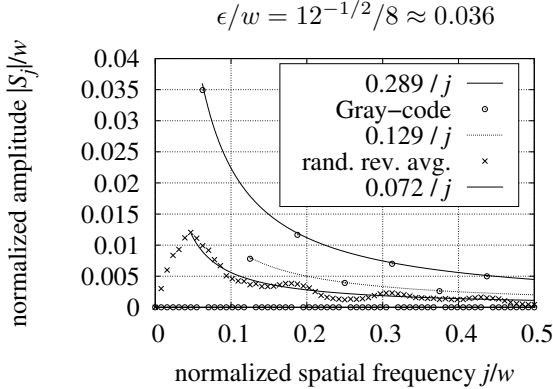


Figure 9 Gray-code eighths spectra

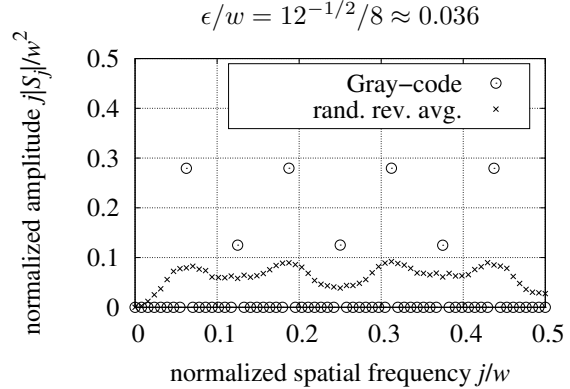


Figure 10 Gray-code eighths spectra

Figure 9 shows spectra of four concatenated repetitions of a Gray-code profile; and the average of the amplitudes of the Fourier spectra of 187 instances of four concatenated random reversal profiles. The peak index j_P of Gray-code eighths is 8 as expected; however the random reversal profiles have $j_P = 6$ because the amplitudes are not correlated between the random eighths. Figure 10 shows that the random reversal amplitudes are spread compared with the isolated Gray-code amplitudes. The effective repeat length for each composite profile is $L_S = L/j_P$.

9. Periodic Roughness

“Uniform roughness” is not compatible with self-similarity; the RMS height-of-roughness of a portion of a self-similar surface must shrink at the succession of scales converging to 0. The existing experimental plates, as well as most manufactured materials consist of repeated patterns of roughness.

A plate with “periodic roughness” is a weakly isotropic array of regions spaced on $L_S \ll L$ centers, each having approximately the same RMS height-of-roughness ϵ . Each patch can be self-similar or not, as long as they have approximately the same height-of-roughness. From the Fourier transform of a measured roughness profile, the effective repeat (wave)length $L_S = L/j_P$, where j_P is the index of the X_j with the largest amplitude.

Sand roughness described in Section 2 is periodic roughness because the sand grains have uniform size and spacing. Similarly for the sphere-roughened plate of Pimenta, Moffat, and Kays[4] described in Section 10. The bi-level plates described by Jaffer in “Convection Measurement Apparatus and Methodology” [10] also have periodic roughness.

For a periodic roughness with $0 < \epsilon < L_S \ll L$ there must be some value of Re below which the flow exhibits laminar or smooth-turbulent behavior along almost the entire length L of the plate. Also, this provides a Re lower-bound for rough-turbulence formulas (16) and (18). The boundary-layer is thinnest at the leading edge. Because the roughness is weakly isotropic, the peak of roughness which disrupts the boundary-layer will occur $L_S/2$ from the leading edge on average. From Schlichting[2], the momentum thickness of laminar and smooth-turbulent boundary-layers are $\delta_2 = 0.664 x Re_x^{-1/2}$ and $\delta_2 = 0.036 x Re_x^{-1/5}$ respectively. With $x = L_S/2 = L/(2j_P)$ and $\delta_2 = \epsilon$, the Re_x thresholds are:

$$Re_L = 0.664^2 2 j_P \left[\frac{L}{2 j_P \epsilon} \right]^2 \quad Re_S = 0.036^5 2 j_P \left[\frac{L}{2 j_P \epsilon} \right]^5 \quad (21)$$

At the $Re_x = Re_L = Re_S$ value where the boundary layer depths are equal:

$$\frac{0.664^2}{0.036^5} = \left[\frac{L}{2 j_P \varepsilon} \right]^3 \quad \frac{L}{\varepsilon} \approx 388 j_P \quad \frac{L_S}{\varepsilon} \approx 388$$

When $L_S/\varepsilon < 388$, the flow transitions directly from laminar to rough-turbulence at Re_L . When $L_S/\varepsilon > 388$, then $Re_S > Re_L$ and the flow transitions from laminar to smooth-turbulence at Re_L , and to rough-turbulence at Re_S . Re_L is the critical Re when $L_S/\varepsilon > 388$. For example, with $L/L_S = 15$ and $L/\varepsilon = 5800$ the critical $Re_L \approx 5 \times 10^5$.

The smooth-turbulent threshold $Re_S \ll 1$ for both bi-level plates and the rough surface tested by Pimenta, Moffat, and Kays[4]. The laminar threshold $Re_L \approx 789$ for the $\varepsilon = 1$ mm bi-level plate. $Re_L = 789$ is too small to test in the Convection Machine wind-tunnel, but Re_L could be measured with a bi-level plate having a smaller height-of-roughness.

Surprisingly, smooth-turbulence can also appear at large Re.

Consider a smooth flat plate etched with a fine square grid of narrow grooves subjected to a moderate flow parallel to its surface. The boundary-layer near the leading edge will be disrupted by the narrow grooves perpendicular to the flow. If this boundary-layer grows to have a momentum thickness larger than ε downstream, then the skin-friction coefficient from that point to the trailing edge will be that for smooth-turbulence: $f_C = 0.037 Re^{-1/5}$. The disrupted flow between the leading edge and transition can't be smooth-turbulence or laminar; Section 3 posits that the only other possibility is rough-turbulence, which would have the skin-friction coefficient of formula (16).

Note that Re_S and Re_L in formulas (21) depend only on the geometry of the plate. If all lengths of the plate are scaled, Re_S and Re_L do not change. Similarly $Re_x = x Re/L$ will be independent of length scaling.

For the Convection Machine[10] bi-level plates the repeat length $L_S = L/26 \approx 11.7$ mm. The top of the posts are $L_T = 8.3$ mm long in the direction of flow. The length variables involved in plate convection are L , L_T , L_S , $L_S - L_T$, x and $\varepsilon = \delta_2$. From convection measurements it appears that $Re_x \propto \varepsilon^{9/4}$ with the other lengths held constant.

There are several conditions under which turbulence should be smooth only; that is accomplished by including dimensionless factors forcing the local Re_ℓ threshold to zero when the post length to post spacing ratio is 0 or 1, or if $\varepsilon = 0$.

$$Re_\ell = \frac{L_S}{L_T} \frac{L_S - L_T}{0.036 L_S} \frac{\varepsilon/2}{L_S - L_T} \frac{L}{0.036 L_S} \left(\frac{\varepsilon}{0.036 L_S} \right)^{5/4} = \frac{L}{0.072 L_T} \left(\frac{\varepsilon}{0.036 L_S} \right)^{9/4} \quad (22)$$

The two bi-level plates tested in the Convection Machine were identical except for their height-of-roughness $\varepsilon = 3$ mm, 1 mm. Correctness of the equation (22) dependence on L_T and L_S is less certain than for ε . The bi-level plate measurements are consistent with the flow transitioning at $Re_x = Re_\ell$ from rough-turbulence to smooth-turbulence. Figure 11 shows excellent agreement between theory and measurement for the 3 mm roughness bi-level plate with the transition at $Re_\ell = 42074$ as calculated by equation (22).

Replacing L_T (the length of each flat) with its maximal possible value L_S gives a Reynolds number upper-bound for the entire periodic plate to be rough-turbulent.

$$Re < \frac{L}{0.072 L_S} \left(\frac{\varepsilon}{0.036 L_S} \right)^{9/4} \approx 24603 \frac{L}{L_S} \left(\frac{\varepsilon}{L_S} \right)^{9/4} \quad \frac{L}{L_S} \gg 1 \quad (23)$$

Note that this worst-case upper-bound (23) is a practical limitation only for surfaces with periodic flat patches like bi-level plates. Other periodic roughness will generate rough-turbulence at large Re.

Combining the bounds (21) and (23):

$$\max \left(0.664^2 \frac{L L_S}{2 \varepsilon^2}, 0.036^5 \frac{L L_S^4}{2^4 \varepsilon^5} \right) < Re < \frac{L}{0.072 L_S} \left(\frac{\varepsilon}{0.036 L_S} \right)^{9/4} \quad \frac{L}{L_S} \gg 1 \quad (24)$$

Disrupted smooth-turbulent boundary-layers aren't laminar or smooth-turbulent; Section 3 posits that the only other possibility is rough-turbulence, implying that when Re is within bounds (24) the flow is rough-turbulent, even for periodic roughness lacking self-similarity.

While the local skin-friction coefficient f_c is not well defined for self-similar roughness, it is tractable for periodic roughness by avoiding the singularity at the leading edge of the plate. It is plotted in Figure 13.

$$\frac{1}{L - L_S} \int_{L_S}^L f_c(x) dx = \frac{1}{3 \ln^2(L/\varepsilon)}$$

$$f_c(x) = \frac{1}{3 \ln^2(x/\varepsilon)} - \frac{2(x - L_S)}{3x \ln^3(x/\varepsilon)} \quad x > L_S \quad x \gg \varepsilon \quad (25)$$

10. Experimental Results

What can be learned from physical measurements of skin-friction or forced-convection from rough plates?

If measurements of plates with isotropic self-similar roughness were close to the predictions of equation (16) or equation (18), then it would support these new formulas for self-similar roughness only. If measurements (over a range of Re values) of diverse plates with periodic isotropic roughness were close to the new predictions, then that would be compelling evidence that these new formulas reflect a physical law of turbulent flow along isotropic surface roughness.

The rough surface tested by Pimenta, Moffat, and Kays[4] was 11 layers of densely packed metal balls 1.27 mm in diameter “arranged such that the surface has a regular array of hemispherical roughness elements.” They use $k_S = 0.79$ mm.

Being repeating patterns, both sphere-roughened and sand-roughened surfaces are self-dissimilar.

The Convection Machine[10] bi-level plate surface was composed of (676) 8.28 mm \times 8.28 mm \times 6 mm posts spaced on 11.7 mm centers. The area of the top of each post was 0.686 cm², half of its 1.37 cm² cell. The RMS height-of-roughness and also the arithmetic-mean height-of-roughness were 3 mm. A periodic equal-area bi-level architecture provides the largest RMS height-of-roughness possible in a 6 mm peak-to-valley span. And this surface has no self-similarity.

Applying convection formula (18) to the bi-level plate yields $Nu = 0.0078 Re Pr^{1/3}$. The corresponding trace “rough turbulent” in Figure 11 matches the “ $\Delta T = 11$ K measured” $\pm 2\%$ from $5500 < Re < 50000$.

At $Re > 50000$ the “post top smooth turbulent” trace (having slope 4/5) shows that convection is from the smooth post tops. The transition at $Re = 42074$ is computed by equation (22). As claimed in Section 9, the convection is rough-turbulent below the $Re = 29751$ upper-bound computed by formula (23).

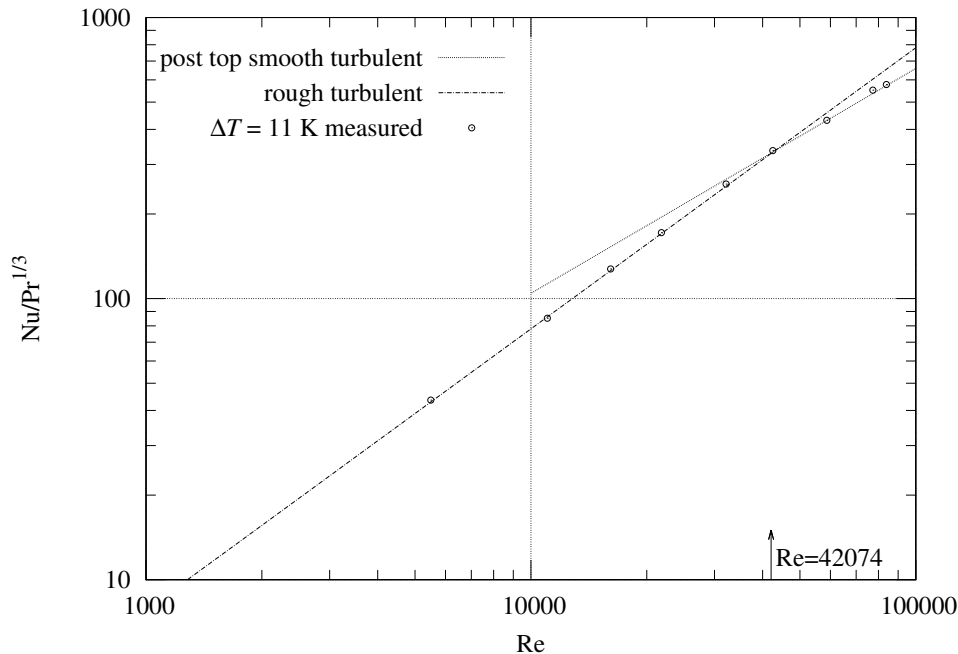


Figure 11 Convection from rough plate

The periodic bi-level plate behaving compatibly with formula (18), which was derived from an analysis of self-similar roughness, supports the claim that formulas (16) and (18) are intrinsic to turbulent flow along isotropic roughness and not specific to self-similar roughness.

11. Fully Rough Regime

Using the 5.33 RMS to sand-roughness conversion factor (from Section 2), Table 1 compares skin-friction coefficients⁷ from three sources at $L/k_S = 100$.

Prandtl-Schlichting (1)	$L/k_S = 100$	$c_f/2 = 0.00838$
Mills-Hang (2)	$L/k_S = 100$	$C_D/2 = 0.00850$
present work (16)	$L/\varepsilon = 5.33$ $L/k_S = 533$	$f_C = 0.00846$

Table 1 Total skin-friction coefficients comparison

Figure 12 shows that the corrected⁸ “.5 Mills-Hang($L/(5.33\varepsilon)$)” formula (2) is within $\pm 1\%$ of equation (16) over the range $100 < L/\varepsilon < 1800$; so it is an improvement compared with the “.5 Prandtl-Schlichting($L/(5.33\varepsilon)$)” formula (1). This close match in the completely rough regime supports the present theory with the measurements from Pimenta, Moffat, and Kays[4] modeled by Mills and Hang[3].

At $L/\varepsilon > 1000$, the inset graph in Figure 12 shows that Mills-Hang, Prandtl-Schlichting, and White differ from the present work, growing to -13% , -18% , and -21% relative to formula (16) ($(1/3) \ln(L/\varepsilon)^{-2}$) at $L/\varepsilon = 10^6$.

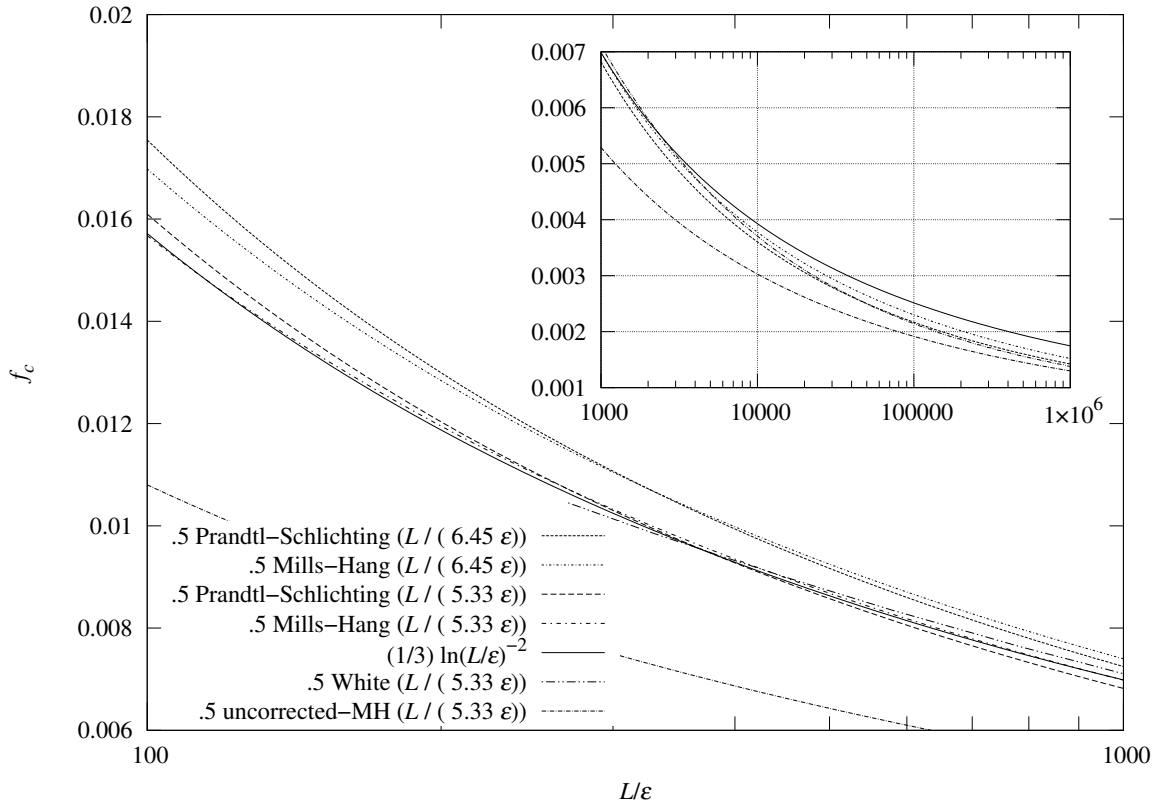


Figure 12 rough-turbulent friction coefficient

⁷ Prandtl and Schlichting[1] calculate τ as $\tau = \rho v_*^2$, not $\tau = \rho v_*^2/2$. This results in Prandtl-Schlichting c_f being twice f_C of the present work. The theoretical development and the tables of measurements in Pimenta, Moffat, and Kays[4] use $C_f/2$, not C_f . In Mills and Hang[3], the tables comparing data from Pimenta, Moffat, and Kays with the Prandtl-Schlichting and Mills-Hang formulas display $C_f/2$ for all three sources.

⁸ See footnote about the Mills-Hang formula in Section 2.

12. Transitional Rough Regime

Afzal, Seena, and Bushra[7] (also Schlichting[2]) relate that the turbulent flow inside commercial pipes behaves differently from the flow inside Nikuradse’s sand coated pipes in the transitional rough regime. While the skin-friction coefficients for commercial pipes are monotonically decreasing with increasing Re on the Moody diagram, in the diagram for Nikuradse’s pipes the coefficient trace for each roughness reaches its minimum just to the right of the smooth skin-friction line, a behavior they term “inflectional”.

The Prandtl-Schlichting plate model apparently inherited the inflectional curve from Nikuradse’s pipes. The total coefficient of resistance (c_f) Moody diagram from Prandtl and Schlichting[1] (also Schlichting[2]) shows c_f following a $-1/5$ slope smooth-turbulent line to a 10% dip spread over a decade of Re just to the right of the smooth-turbulent line before leveling out further to the right.

For a self-similar roughness (producing turbulence) there should be no variation in skin-friction coefficient with Re.

Pimenta, Moffat, and Kays write that, while the agreement of their data with the Prandtl-Schlichting plate model is “rather good” in the fully rough regime, their apparatus does not have the same behavior as “Nikuradse’s sand-grain pipe flows in the transition region”.

Prandtl and Schlichting put the boundary between the transitional rough and fully rough regimes for a plate at “roughness Reynolds number” $Re_k = v*k/\nu = 70.8$. Pimenta, Moffat, and Kays put it at $Re_k = 65$. Solving for Re:

$$Re_k = v*k/\nu = \frac{v}{\sqrt{3} \ln(L/\varepsilon)} \frac{5.33 \varepsilon}{\nu} = \frac{5.33 Re}{\sqrt{3} (L/\varepsilon) \ln(L/\varepsilon)}$$

$$Re \approx 0.325 Re_k \frac{L}{\varepsilon} \ln \frac{L}{\varepsilon} \quad (26)$$

Figure 13 shows the local skin-friction coefficient versus x/k_S for the Pimenta, Moffat, and Kays sphere-roughened plate at three rates of flow, $Re_k = 41.6, 68.5,$ and 103 . The averages of these local coefficients⁹ (from $450 < x/k_S < 2800$) are $C_D = 0.00247, 0.00252,$ and 0.00253 respectively. These C_D values are within 2.5% of each other, significantly less than the 10% spread predicted by Prandtl and Schlichting. The “Mills-Hang fully rough” trace is the local $C_f/2$ fit by Mills and Hang.

The small dependence of C_D on Re for this periodic surface supports the new theory for periodic roughness more than it supports the Prandtl-Schlichting theory.

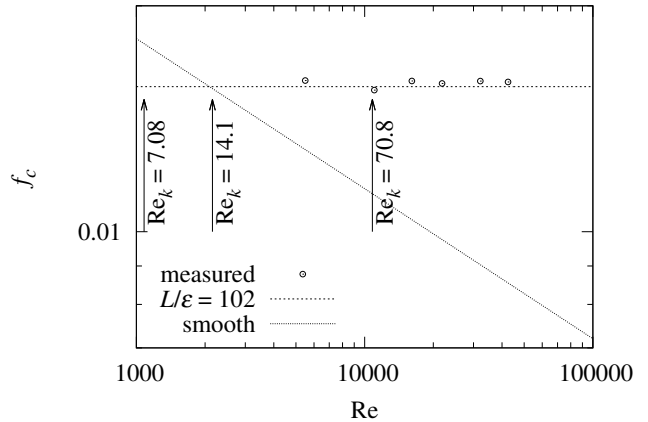
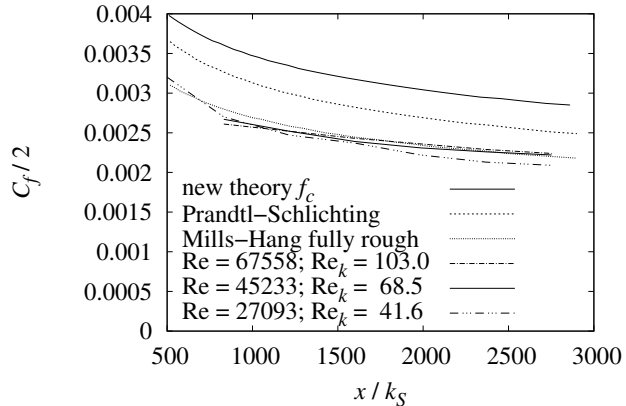


Figure 13 Local C_f of sphere-roughened plate

Figure 14 f_C vs. Re of bi-level plate

Figure 14 is a Moody diagram of the 3 mm RMS roughness bi-level plate measurements converted to friction coefficients f_C using the Chilton and Colburn J-factor analogy (17), and arrows showing the Prandtl-Schlichting regime boundaries calculated using equation (26). The “measured” points are within $\pm 2\%$ of the “ $L/\varepsilon = 102$ ” line at $f_C = 0.0156$ and are level within their expected measurement uncertainties. Not shown in Figure 14 are convection measurements at $Re < 5500$ which are mixed with natural convection for which the analogy doesn’t apply.

⁹ $C_f/2$ at $x/k_S = 452$ was measured only at $Re_k = 41.6$; it is included in all three averages.

Figure 15 shows the whole range of convection measurements on both the 3 mm and 1 mm roughness plates. Of interest is that, even with natural convection mixed in, there are two measurements of the 1 mm plate which are below the “smooth turbulent asymptote” trace. On the Moody chart these points would be to the left of the smooth turbulent trace. So not only is there no transition at $Re_k = 70.8$, the smooth versus rough turbulence transition is not at $Re_k = 14.1$; equations (21) predict lower Re transition values.

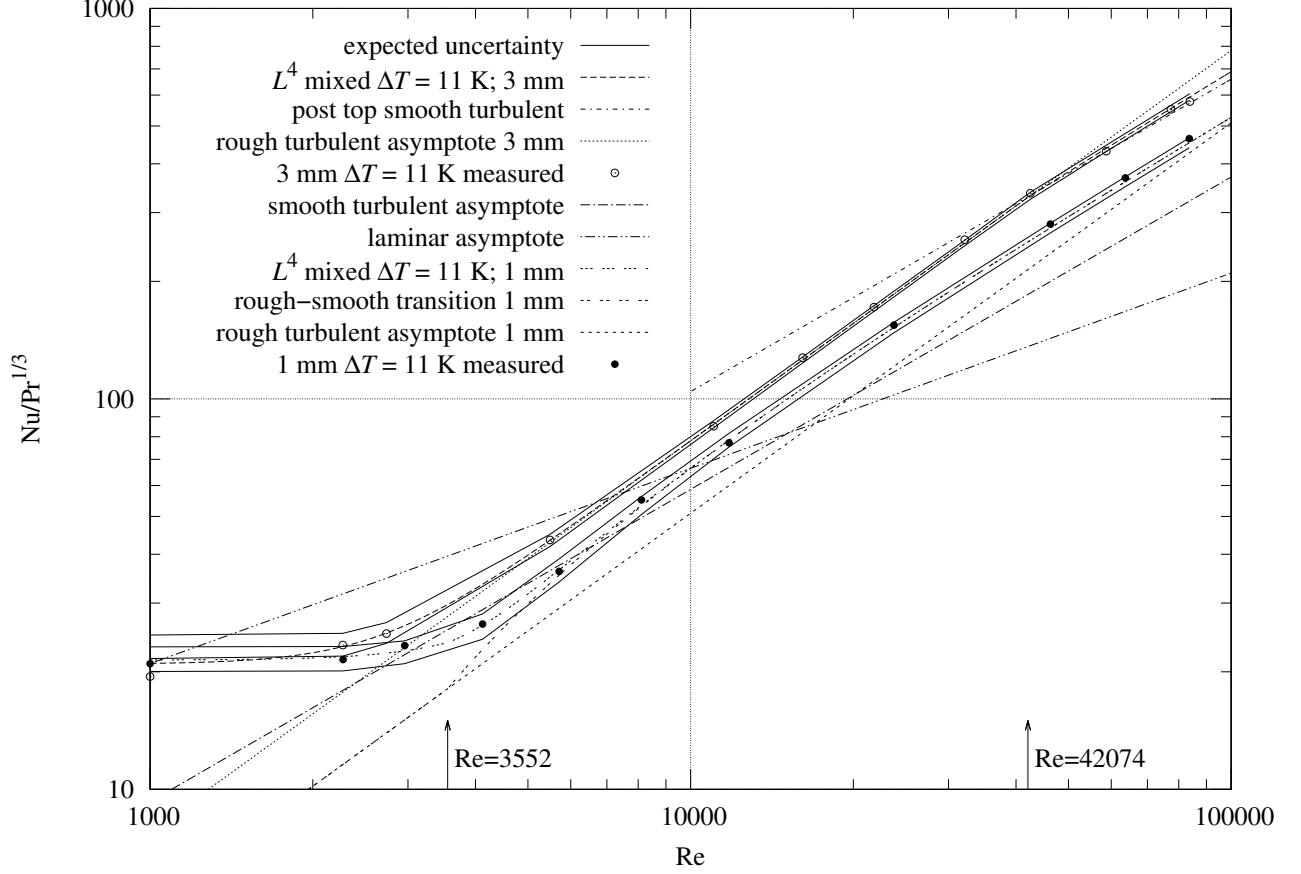


Figure 15 Convection from rough plate

13. Conclusions

- For a periodic or self-similar plate surface with isotropic RMS height-of-roughness $\varepsilon > 0$ which is producing rough-turbulence in a steady flow of strength Re , the skin-friction coefficient and total forced convection formulas are:

$$f_C = \frac{1}{3 \ln^2(L/\varepsilon)} \quad Nu = \frac{Re Pr^{1/3}}{6 \ln^2(L/\varepsilon)} \quad \frac{L}{\varepsilon} \gg 1$$

- For periodic isotropic roughness with period $L_S \ll L$, the flow will be rough-turbulent (to which the formulas apply) when:

$$\max\left(0.664^2 \frac{L L_S}{2 \varepsilon^2}, 0.036^5 \frac{L L_S^4}{2^4 \varepsilon^5}\right) < Re < \frac{L}{0.072 L_S} \left(\frac{\varepsilon}{0.036 L_S}\right)^{9/4} \quad \frac{L}{L_S} \gg 1$$

- For periodic isotropic roughness with $L_S/\varepsilon > 388$ the critical Re is:

$$Re_L = 0.664^2 \frac{L L_S}{2 \varepsilon^2} \quad \frac{L_S}{\varepsilon} > 388 \quad \frac{L}{L_S} \gg 1$$

Acknowledgments

The idea of self-similar roughness grew out of a discussion with Nina Koch about turbulence self-similarity. Thanks to John Cox and Doug Ruuska for machining the bi-level plates.

14. Nomenclature

	Nu = total Nusselt number (convection)
	Pr = fluid Prandtl number
	Re = Reynolds number of flow parallel to the plate
	Re _ℓ = local Reynolds number threshold
Re _k = v* k/ν	= roughness Reynolds number
	Re _L = laminar Reynolds number upper-bound
	Re _S = smooth-turbulent Reynolds number upper-bound
Re _x = x Re/L	= local Reynolds number
	C _D = Mills and Hang total friction coefficient
	C _f /2 = Pimenta, Moffat, and Kays local friction coefficient
	c _f = Prandtl and Schlichting total friction coefficient
	f _c = local friction coefficient
	f _C = total friction coefficient
G(x, w)	= Gray-code profile function
j _P	= index of largest X _j
k _S	= sand-roughness (m)
L	= plate characteristic-length (m)
L _S	= effective roughness repeat length (m)
L _T	= post length in direction of flow (m)
n	= branching factor of profile roughness function
S _j	= corrected discrete Fourier transform coefficient
v	= bulk fluid velocity (m/s)
v*	= friction velocity (m/s)
w = 2 ^ν	= integer power of two
W(x, w)	= wiggliest integer self-similar profile
Y(x, w)	= integer ramp-permutation self-similar profile
X _j	= discrete Fourier transform coefficient
x, y	= distance (m)
z(x)	= profile roughness function (m)
z̄	= mean height of roughness (m)
Z	= profile roughness function random variable (m)

Greek Symbols

	δ ₂ = momentum boundary-layer depth (m)
	ε = RMS profile height-of-roughness (m)
	ε = RMS surface height-of-roughness (m)
ν = log ₂ w	= positive integer
	ρ = fluid density (kg/m ³)
	τ = fluid shear stress (N/m ²)

15. References

- [1] L. Prandtl and H. Schlichting. *The Resistance Law for Rough Plates*. Translation (David W. Taylor Model Basin). Navy Department, the David W. Taylor Model Basin, 1934. Translated 1955 by P.S. Granville.
- [2] Hermann Schlichting, Klaus Gersten, Egon Collaborateur. Krause, Herbert Collaborateur. Oertel, and Katherine Mayes. *Boundary-layer theory*. Springer, Berlin, Heidelberg, Paris, 2000. Corrected printing 2003.
- [3] A. F. Mills and Xu Hang. On the skin friction coefficient for a fully rough flat plate. *J. Fluids Eng*, 105(3):364–365, 1983.
- [4] M. M. Pimenta, R. J. Moffat, and W. M. Kays. *The Turbulent Boundary Layer: An Experimental Study of the Transport of Momentum and Heat with the Effect of Roughness*. Department of Mechanical Engineering, Stanford University, 1975.
- [5] Frank White. *Viscous Fluid Flow, 3rd Edition*. McGraw-Hill, 2006.
- [6] Karen A Flack, Michael P Schultz, Julio M Barros, and Yechan C Kim. Skin-friction behavior in the transitionally-rough regime. *International Journal of Heat and Fluid Flow*, 61:21–30, 2016.
- [7] Noor Afzal, Abu Seena, and A. Bushra. Turbulent flow in a machine honed rough pipe for large reynolds numbers: General roughness scaling laws. *Journal of Hydro-environment Research*, 7(1):81–90, 2013.
- [8] J.H. Lienhard, IV and J.H. Lienhard, V. *A Heat Transfer Textbook*. Phlogiston Press, Cambridge, MA, 5th edition, 2019. Version 5.00.
- [9] Mitchell G. Newberry and Van M. Savage. Self-similar processes follow a power law in discrete logarithmic space. *Phys. Rev. Lett.*, 122:158303, Apr 2019.
- [10] A. Jaffer. Convection measurement apparatus and methodology, 2019. [Online; accessed 25-October-2019].